IAES International Journal of Artificial Intelligence (IJ-AI)
Vol. 15, No. 1, February 2026, pp. 412~428
ISSN: 2252-8938, DOI: 10.11591/ijai.v15.i1.pp412-428

Robust UAV localization of ground sensors in urban environments via path loss refinement and geometric selection

Ahmed M. A. A. Elngar[1], Heng Siong Lim[1], Yee Kit Chan[1], Yaser Awadh Bakhuraisa[1], Ida Wahidah[2]
[1]Faculty of Engineering and Technology, Multimedia University, Melaka, Malaysia
[2]School of Electrical Engineering, Telkom University, Bandung, Indonesia

Article Info

Article history:

Received Oct 2, 2025
Revised Jan 15, 2026
Accepted Jan 22, 2026

Keywords:

Geometric selection
Localization
Path loss
Unmanned aerial vehicles
Urban environment

ABSTRACT

Localizing ground sensors with unmanned aerial vehicles (UAVs) in dense urban environments is challenging because multipath and non-line-of-sight (NLoS) propagation distorts path loss (PL) measurements. This paper proposes a two-stage UAV localization framework that refines PL data and selects geometrically stable waypoint subsets before position estimation. In stage 1, PL samples are spatially smoothed by averaging measurements at neighboring UAV waypoints to reduce localized fluctuations. In stage 2, waypoint subsets are filtered using non-collinearity and non-adjacency constraints, and sensor positions are estimated using weighted least squares (WLS) and particle swarm optimization (PSO), with final estimates averaged across valid subsets. Wireless InSite ray-tracing simulations show that the framework reduces mean absolute error (MAE) from over 150 m to approximately 8.5 m. The proposed approach improves the practicality of UAV-assisted localization for urban internet of things (IoT) sensor deployments.

Corresponding Author:

Heng Siong Lim
Faculty of Engineering and Technology, Multimedia University
St. Ayer Keroh Lama, Melaka 75450, Malaysia
Email: hslim@mmu.edu.my

1. INTRODUCTION

Unmanned aerial vehicles (UAVs) have become popular in recent years, attracting growing interest from both industry and academia as a promising solution for a wide range of applications. Due to their ability to navigate complex urban structures, they have been utilized for localization purposes to overcome challenges arising from global positioning system (GPS) signal blockage. In such scenarios, the UAV utilizes communication channel parameters to estimate the ground sensors' locations [1].

In general, localization techniques can be classified into several categories. Range-based methods estimate positions using signals' propagation characteristics such as time of arrival (ToA), angle of arrival (AoA), and received signal strength indicator (RSSI) or path loss (PL), which provide distance or angle information between nodes. In contrast, range-free methods do not rely on precise physical measurements; instead, they use network connectivity to estimate locations. Another method is fingerprinting-based localization, which involves collecting signal features like RSSI at known reference locations to build a database and then matching real-time data to this database to estimate the unknown position. While range-free methods are simple, they typically suffer from low localization accuracy due to their sole dependency on connectivity information without exploiting physical signal properties. Therefore, range-based methods are preferred for ground sensor localization in urban environments using a UAV [2].

For resource-constrained internet of things (IoT) applications, such as ground sensors, RSSI-based methods are widely regarded as the most suitable solution for localization due to their low cost, minimal hardware requirements, and energy efficiency [3]. However, their effectiveness in urban environments is significantly challenged by strong signal fluctuations caused by dense multipath reflections and obstructions, which can severely degrade localization accuracy. The most popular solution to address these challenges is calibrating the parameters of the PL model using a curve-fitting technique. However, this technique often proves insufficient in practice, since the standard PL model cannot capture the complex variations and distortions in RSSI/PL measurements caused by multipath propagation and environmental dynamics in dense urban settings. As a result, this leads to significant errors in distance estimation and, consequently, poor localization accuracy [4].

To address this issue, this work proposes a two-stage localization framework to minimize PL measurement errors and enhance localization accuracy. In the first stage, the PL measurements are refined to reduce errors caused by multipath effects, thereby improving distance estimation accuracy. In the second stage, subsets of UAV waypoints are selected from the entire waypoint set to compute the ground sensor's location. The waypoint combinations are based on the well-known geometric dilution of precision (GDOP) criterion [5]. The final localization estimate is then obtained by averaging the solutions from all selected combinations. Overall, the proposed two-stage approach improves the reliability of PL measurements and enhances localization accuracy by leveraging both spatial and geometric insights. The two-stage proposed framework is illustrated in Figure 1.

i) Stage 1: collect PL at UAV waypoints → apply spatial refinement → fit/calibrate log-distance PL model (parameters using reference node).
ii) Stage 2: generate waypoint subsets under geometric constraints (non-collinear, non-adjacent) → run weighted least squares (WLS)/particle swarm optimization (PSO) multilateration → average estimates.

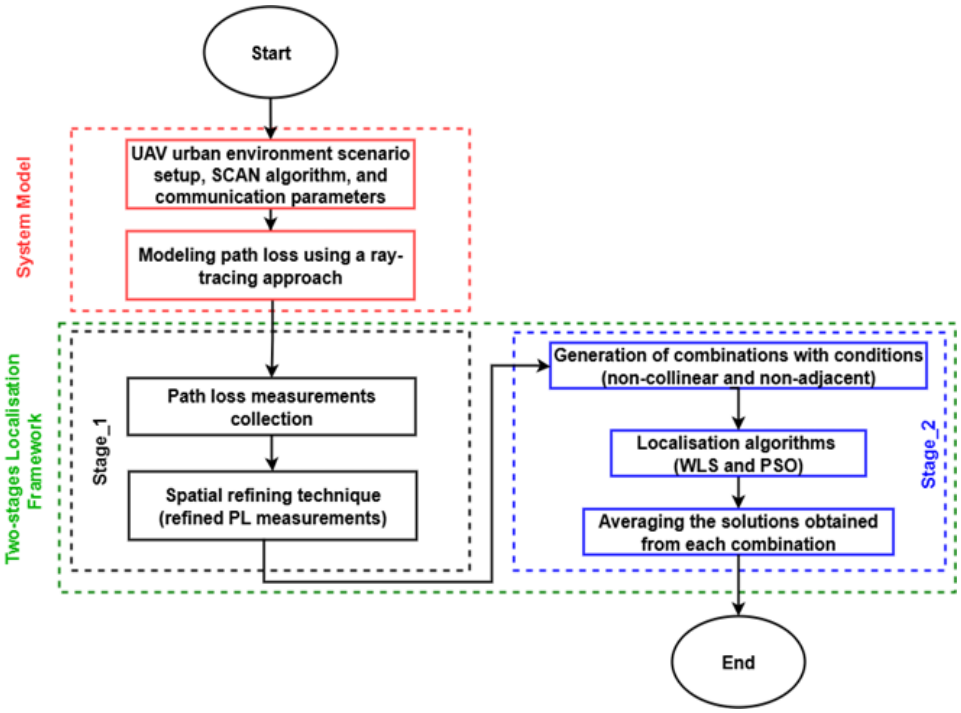

Figure 1. Proposed two-stage localization framework

The novel contributions of this work are summarized as follows:

i) A spatial-based refinement technique is introduced to reduce PL measurement error by leveraging the spatial coordinates of waypoints. The refined PL at each waypoint is computed as the average of its own PL measurement and those of its spatial neighbors.
ii) A waypoint selection scheme is developed to improve the localization accuracy of multilateration algorithms. The scheme, guided by the well-known GDOP principle, operates in two steps: i) selecting non-collinear waypoints and ii) selecting non-adjacent waypoints from the subset obtained in the first step.

The remainder of this paper is organized as follows: section 2 reviews related works, while section 3 outlines the system model. Sections 4 and 5 present the preliminaries and the spatial-based refinement technique. Section 6 details the localization algorithm, covering the waypoint selection scheme and location estimation. Section 7 describes the simulation environment setup. Section 8 discusses the results. Finally, section 9 concludes the paper.

2. RELATED WORKS

Recently, studies have proposed to utilize RSSI as a parameter for localization to estimate the target's location. According to Teeda *et al.* [6], RSSI measurements obtained by UAV at 865 MHz over open farmland was used to estimate the target's location. The path loss exponent (PLE) was assumed to be fixed value near-free-space. On the other hand, Aamir and Ali [7] have investigated the utilization of PL measurements of long range (LoRa) technology along with [8] using 915 MHz for localization. At 3.9 GHz, air-to-ground surveys above mixed woodland–suburb blocks still enjoyed largely line-of-sight conditions with only moderate extra loss [9]. Similarly, Ahmad *et al.* [10] RSS measurements at 5.9 GHz have been used to estimate the positions of the target nodes that were near line of sight (LoS) condition.

Higher carrier frequencies are often required for modern IoT applications to support high data rates. However, a key challenge in RSSI-based localization is the large measurement error observed at higher frequencies, particularly in dense multipath environments such as urban areas [11]. Existing approaches can be broadly categorized into: i) treating key PL parameters (e.g., PLE and transmit power) as unknown and estimating them jointly with the position and ii) assuming fixed values for these parameters. For example, Jin *et al.* [12] treats the PLE as an unknown random state that is jointly inferred with the node position, while Najarro *et al.* [13] jointly estimates position, transmit power, and PLE using differential evolution. Similarly, Mukhopadhyay and Alouini [14] cooperative localization techniques (with unknown parameters) (CTUP) system in [15] estimate node position and transmit power jointly. Liu *et al.* [16] presented piecewise-convex approximation localization (PCAL) to investigate the ability of UAV to localize a mobile station (MS) using RSSI measurements at 2.4 GHz. The PCAL was used to calculate the location of MS and unknown PLE.

Although jointly estimating these parameters can improve localization accuracy, it significantly increases computational complexity. To reduce this complexity, several works assume that the PL parameters are known. For instance, Cheng *et al.* [17] assumes fixed PL parameters, while Li *et al.* [18] exploits known distances between trajectory points to compute PL parameters and improve localization accuracy. Likewise, Chu *et al.* [19] uses a fixed PLE with expectation-maximization, and Wang *et al.* [20] applies semidefinite programming with a fixed PLE. However, assigning fixed parameter values remains challenging because PL parameters are environment-dependent. There are several methods that have been proposed to tackle this issue.

However, Kumar *et al.* [21] solved the self-localization problem using RSSI measurements as well as the anchor positions information by utilizing the solution of WLS. Moreover, Hu *et al.* [22] proposed an ultra-wideband (UWB) positioning framework for non-line-of-sight (NLoS) scenarios using WLS based on reference sensor and using ray-tracing to convert NLoS into LoS environment. Subsequently in [23], a trilateration algorithm for using RSSI for localization avoiding the no uniqueness of a solution by minimizing the error function and using Taylor series approximation. Research by Prasad and Bhargava [3], two-step linear least squares (TLLS) solution is proposed for distance estimation, then estimating the location and the PLE as well. Research by Kang *et al.* [24], a target localization algorithm based on hybrid RSSI/AoA measurements is proposed using error covariance WLS (ECWLS) algorithm and comparing it with WLS and other loss functions.

Esrafilian *et al.* [25] proposed a hybrid channel model to improve the localization accuracy. In such model, the PSO was used to optimize the parameters of channel model at 5 GHz. Although the accuracy is improved using this method compared to his previous work [26], the drawback of this method is the required data collected at known locations to train the model which is unavailable in some scenarios. Subsequently in [27], hierarchical reference particle swarm optimization (HRPSO) was proposed to improve the performance of PSO utilized in UAV localization. Moreover in [10], the PL parameters have been calculated using the least square technique. However, this technique is suspected to be affected by PL measurements outliers. Research by Yang [28], PSO algorithm is proposed in different types such as self-adaptive inertia weight particle swarm optimization (SAPSO) and improved self-adaptive inertia weight particle swarm optimization (ISAPSO).

To overcome this issue, we propose a PL refining method to address the fluctuations caused by multipath effects from inevitable dense reflections in urban environments. Based on the refined PL, the model parameters are then determined and subsequently utilized for deriving the ranging model to estimate the distance and location. Table 1 summarizes the most closely related UAV-assisted RSSI/PL localization studies, highlighting their key assumptions and limitations in comparison with the proposed framework.

Table 1. Summary of closely related UAV-assisted RSSI/PL localization studies

Ref.	Frequency	Methodology	Parameter assumptions	Key outcome/limitation
[7]	915 MHz	RSSI→distance + trilateration	Log-distance/log-normal shadowing; fitted PLE reported	Reports fitted PLE values; limited quantitative urban benchmarking and no MPC mitigation pipeline
[8]	3.9 GHz	Channel measurement + ray-tracing comparison	Reports PLE/σ and discusses two-ray effects; channel modelling emphasis	Provides PL/shadowing baselines; not an end-to-end localization framework under severe MPC
[20]	5 GHz	PSO + hybrid channel model (map/learning aided)	Hybrid LoS/NLoS modelling; often needs training/map context	Improves accuracy in urban settings; depends on model tuning/training and/or map context
Proposed	5.9 GHz	Two-stage: spatial PL refinement + constrained subset selection + WLS/PSO	Targets urban MPC/NLoS without 3D maps/training; refinement + geometry constraints before estimation	Reduces error from >150 m to ~8.5 m; designed specifically for dense-urban PL distortion

3. SYSTEM MODEL

This section elaborates on system model as is illustrated in Figure 2. In this model, S ground sensors are randomly distributed within an outdoor urban environment at locations $P_s = [x_s, y_s], s = 1, 2, \dots, S$. One sensor serves as a known reference point (shown as a green square), while the locations of the remaining sensors are unknown and must be determined (shown as red squares). These ground sensors periodically emit signals that are captured by a UAV. The UAV navigates a predetermined trajectory generated by the systematic coverage area navigation (SCAN) algorithm at a constant altitude, a method well-suited for systematic area coverage [29]. While flying along this path (shown as a black dotted line), the UAV stops at N waypoints with known locations $WP_i = [\, x_i, y_i], i = 1,2, \dots, N$, (shown as black circles), to collect PL measurements.

In this work, the PL data is obtained using a ray-tracing technique implemented in wireless insite [30] to ensure a high-fidelity representation of the complex propagation environment. The data collected from the known reference sensor is used to optimize the parameters of the PL model, as explained in section 5. This optimized model is then used to estimate the distance between the UAV and the unknown ground sensors. Subsequently, the locations of the unknown sensors are calculated using the optimization methods detailed in section 6.

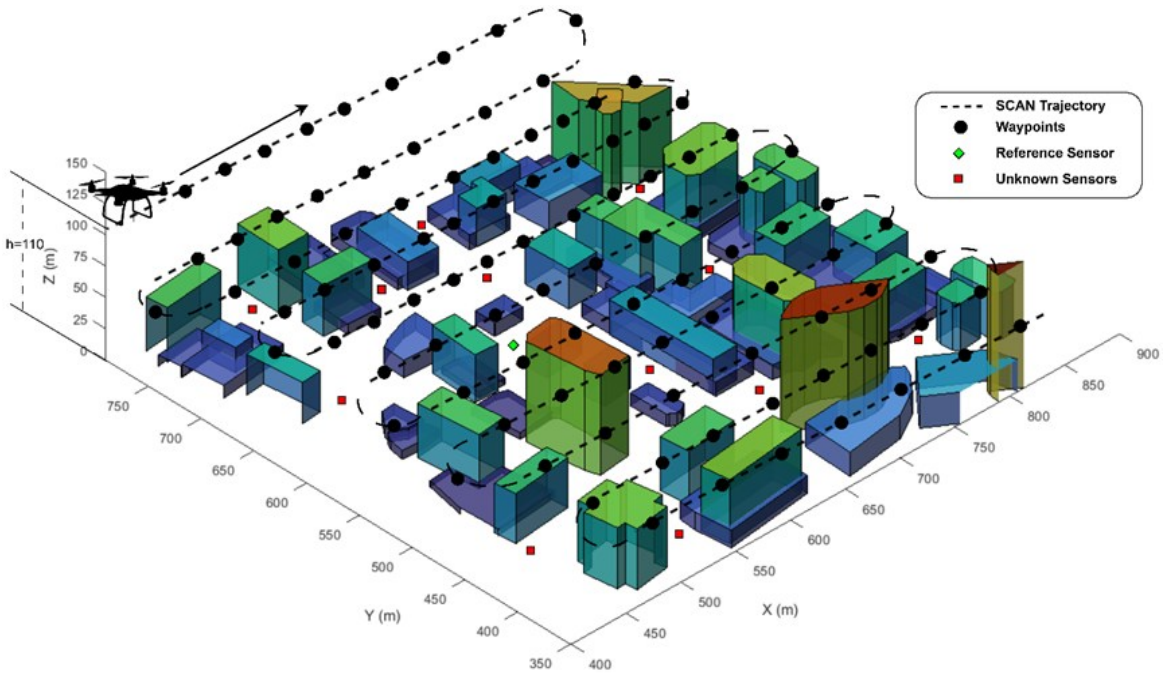

Figure 2. System model overview

4. PRELIMINARIES

This section explains the preliminaries of the PL model used to relate signal strength to the distance between the UAV and a ground sensor. The PL at the *i*-th waypoint is computed as (1).

$$PL_i = P_t - RSSI_i \quad (1)$$

Where P_t is the sensors transmit power in dBm, and $RSSI_i$ is the received power at the i-th waypoint in dBm. This formulation assumes that antenna gains, and other system losses are already accounted for.

The relationship between this measured PL and distance is widely described by the log-distance PL model [31], which is expressed as (2).

$$PL(d_i) = PL(d_0) + 10\beta.\log_{10}\left(\frac{d_i}{d_0}\right) \quad (2)$$

Where $PL(d_i)$ denotes the measured PL at distance d_i, and $PL(d_0)$ is the reference PL at a close-in reference distance ed_0. Theoretically the $PL(d_0)$ can be theoretically calculated using the free-space path loss (FSPL) formula as shown in (3). The parameter β is PLE. The PLE is a critical, environment-dependent parameter that must be determined to ensure accurate distance estimation. The FSPL formula is given by (3).

$$PL(d_0) = 20\ \log_{10}(\mathrm{f}) + 32.44 \quad (3)$$

Where f is the carrier frequency in GHz.

5. SPATIAL-BASED REFINEMENT TECHNIQUE

This section explains how the raw PL data is processed to reduce errors caused by multipath components (MPC). While a Kalman filter is often used to refine PL measurements, it is not suitable for this scenario. The stationary nature of the reflectors (buildings) means that PL samples collected at the same waypoint are identical, violating the assumption of independent measurement noise that a Kalman filter relies on. To overcome this issue, this work employs a spatial-filtering approach. In this method, the PL value at a specific waypoint is replaced by a weighted average of itself and its immediate physical neighbors. This technique is justified by the physical properties of the channel; PL is spatially correlated, meaning adjacent waypoints are expected to have similar large-scale signal characteristics. By averaging nearby measurements, the filter effectively smooths out localized, random errors caused by small-scale MPCs.

After the raw PL data has been refined using this spatial filter, the parameters of the log-distance model are determined using the data from the known reference sensor. A linear least-squares regression is performed on the smoothed PL data to find the optimal values for the reference PL $PL(d_0)$ and the PLE β that create a linear fit for the log-distance model by solving the following minimisation problem.

$$\left[\widehat{PL}(d_0), \hat{\beta}\right] = \arg\min_{PL(d_0),\beta} \sum_{i=1}^{N} \left(PL_i - \left(PL(d_0) + \beta \cdot 10\log_{10}\left(d_i/d_0\right)\right)\right)^2 \quad (4)$$

This provides an accurate PL model tailored to specific environment before it is used for distance estimation.

6. LOCALIZATION ALGORITHM

This section details the localization algorithm, which processes the estimated ground distances to determine the final 2D coordinates of each unknown sensor as shown in Algorithm 1. The process is fundamentally based on the principle of multilateration, where multiple known UAV waypoint positions and their respective distances are used to find an unknown position. A crucial pre-processing step, waypoint combination selection, is first applied to select geometrically stable sets of waypoints. These selected waypoints (SWP) are then fed into the main localization algorithms for the final position calculation.

Algorithm 1. Two-stage UAV localization framework
Inputs: waypoint set and coordinates, PL measurements, reference node data, thresholds/constraints.
1) Acquire PL measurements along SCAN waypoints.
2) Stage 1: spatial refinement (neighbor averaging).
3) Fit/calibrate log-distance PL parameters using reference node.
4) Convert PL → distance estimates for unknown sensors.
5) Stage 2: generate waypoint subsets satisfying (non-collinear, non-adjacent).
6) For each subset: estimate position via WLS or PSO.
7) Average/aggregate all valid subset solutions → final estimate.
Outputs: estimated sensor position(s).

6.1. Waypoint combination generation

Initially, a set of the n most suitable waypoints, denoted SWP, is created. This is achieved by first estimating the 3D slant distance from the unknown sensor to every available UAV waypoint. Then, only the waypoints whose estimated distance falls within a predefined range are included in the SWP set. This filtering step is designed to exclude waypoints that are either too close (which may suffer from near-field effects) or too far away (which are more susceptible to severe measurement inaccuracies), thereby retaining only the most reliable data for localization.

The geometric configuration of the UAV waypoints relative to the unknown sensor is a crucial factor that greatly affects the final localization accuracy. This relationship is formally measured by a metric called dilution of precision (DOP), which indicates how the waypoint geometry impacts the accuracy of the position estimate. Statistically, DOP acts as a multiplier of the ranging error; a lower DOP value signifies a more favorable geometric arrangement and thus a greater potential for accurate localization. For the 2D localization problem, the horizontal dilution of precision (HDOP) is utilized. It is derived from a geometry matrix, denoted as H, constructed as (5) [5].

$$H = \begin{bmatrix} \frac{(x_s - x_1)}{r_{1-\,actual}} & \frac{(y_s - y_1)}{r_{1-\,actual}} \\ \frac{(x_s - x_2)}{r_{2-\,actual}} & \frac{(y_s - y_2)}{r_{2-\,actual}} \\ \vdots & \vdots \\ \frac{(x_s - x_N)}{r_{N-\,actual}} & \frac{(y_s - y_N)}{r_{N-\,actual}} \end{bmatrix} \quad (5)$$

Where (x_s, y_s) are the coordinates of the unknown sensor, (x_i, y_i) for $i = 1, .., N$ are the coordinates of the i-th waypoint, and $r_{i-actual}$ is the true 2D ground distance between them. The covariance matrix G is then derived as (6).

$$G = (H^T H)^{-1} \quad (6)$$

From which HDOP can be computed from the diagonal elements of this covariance matrix. Specifically, it is the square root of the sum of $G_{1,1}$ which represents the variance of the error in the x-coordinate, and $G_{2,2}$ which represents the variance of the error in the y-coordinate as (7).

$$HDOP = \sqrt{G_{1,1} + G_{2,2}} \quad (7)$$

A direct calculation of HDOP for each potential waypoint combination is impractical, as the formula for the geometry matrix H requires the unknown sensor coordinates (x_s,y_s). Therefore, this work uses the HDOP concept as a guiding principle to establish two practical geometric conditions that ensure a well-conditioned matrix and a low HDOP value without needing to solve this circular problem. The stability of the HDOP calculation depends entirely on the properties of the matrix product ($H^T H$). A high HDOP is the direct result of this matrix being singular or ill-conditioned. The proposed geometric rules are designed to prevent this:

i) The non-collinear condition: if waypoints are collinear (on a straight line), the geometry provides ranging information in only one dimension. This causes the geometry matrix H to become rank-deficient, which in turn makes the ($H^T H$) matrix singular (non-invertible). Mathematically, this corresponds to an infinite HDOP. The non-collinear rule is therefore a direct safeguard to eliminate these geometrically unstable combinations.

ii) The non-adjacent condition: if waypoints are clustered closely together, the directional vectors in the rows of matrix H become very similar. This causes the ($H^T H$) matrix to be ill-conditioned (nearly singular). Inverting an ill-conditioned matrix is a numerically unstable process that significantly amplifies any small measurement errors, resulting in a large HDOP. The non-adjacent rule ensures that waypoints are well-spread, leading to a well-conditioned matrix and a low, stable HDOP.

Following the principles of multilateration, all possible combinations of four waypoints are then generated from this SWP set. The total number of these candidate subsets, m, is given by $m = \binom{SWP}{4}$. Each candidate subset, denoted as $C \in R^{4\times 2}$, is a matrix and must be a subset of SWP, expressed as (8).

$$C \subseteq SWP \text{ and } |C| = 4 \quad (8)$$

After the candidate subsets are generated, each candidate is evaluated to ensure it has a suitable geometry that satisfies both non-collinear and non-adjacent conditions.

The non-collinearity condition is critical for a stable localization result, as it ensures the waypoints are well-spread and are not on a single line. This is satisfied by verifying that the area of the triangle formed by any three waypoints within the candidate subset is significantly greater than zero. For any three points (x_1, y_1), (x_2, y_2), and (x_3, y_3) in the subset, the area must satisfy as (9).

$$Area = \frac{1}{2}x_1|(y_2 - y_3) + x_2(y_3 - y_1) + x_3(y_1 - y_2)| > \epsilon_{area} \quad (9)$$

Where ϵ_{area} is a small positive threshold used to reject nearly collinear waypoint triplets, not only perfectly collinear ones. In practice, measurement noise and limited numerical precision can produce very small triangle areas even when points are not exactly on a single line. Therefore, ϵ_{area} is selected relative to the waypoint spacing used in the SCAN spacing, so that degenerate or near-degenerate geometries are excluded while keeping the majority of well-spread triplets valid. This improves the conditioning of multilateration and stabilises the localization solution.

The non-adjacency condition is then applied to ensure the waypoints in a candidate subset are not clustered together, which improves the geometric strength of the multilateration. This is enforced by requiring the Euclidean distance between any two waypoints, WP_i and WP_j, in the subset to be greater than a minimum separation threshold, d_{thresh} as (10).

$$d(WP_i, WP_j) > d_{thresh} \quad (10)$$

Where i and j are waypoint indices. The threshold d_{thresh} is set with respect to the waypoint spacing used in the SCAN grid to prevent clustered subsets. Specifically, d_{thresh} is chosen slightly larger than the diagonal-neighbour separation (approximately $\sqrt{2}$ times the SCAN waypoint spacing), so that immediate horizontal, vertical, and diagonal neighbours are excluded. This increases the effective baselines between SWP, improves geometric diversity, and reduces sensitivity to small distance-estimation errors.

In cases where waypoints are indexed sequentially along the flight path, a computationally simpler method can be used by requiring that indices of any two waypoints are not consecutive as shown in (11).

$$|index(WP_i) - index(WP_j)| > 1 \quad (11)$$

Finally, a candidate subset C of four waypoints is included in the final set of valid subsets, C_{valid}, only if it simultaneously satisfies both geometric conditions.

In (12), let $\binom{C}{k}$ denotes the set of all *k*-element subsets of C.The non-collinearity condition requires $C_{valid} \subseteq C$ to satisfy the condition $Area(T) > \epsilon_{area}$, for all $T \in \binom{C}{3}$. At the same time, the non-adjacency condition mandates that $d(P) > d_{thresh}$ for all $P \in \binom{C}{2}$. Both of these geometric constraints must hold true for the subset to be considered valid. In other words:

$$\begin{aligned} &Area(T) > \epsilon_{area}, \forall T \in \binom{C}{3} \\ &d(P) > d_{thresh}, \forall P \in \binom{C}{2} \end{aligned} \quad (12)$$

where C_{valid} is the final set containing all valid subsets.

6.2. Ground sensor localization

For an unknown sensor, let the actual 2D position be denoted by $p_s = [x_s, y_s]$. Its estimated position by $\hat{p}_s = [\hat{x}_s, \hat{y}_s]$. The estimation is carried out using the PL measurements obtained from N known UAV waypoint locations. First, the 3D slant distance $\hat{d}_i$ from the unknown sensor to the i-th waypoint is estimated using the PLE, $\hat{d}_i$, determined from the reference sensor data via the log-distance model. In the (13) gives estimated 3D slant distance.

$$\hat{d}_i = d_0 . 10^{\left(\frac{PL(d_i) - PL(d_0)}{10\beta}\right)} \quad (13)$$

Next, the estimated 3D slant distance is converted to the estimated 2D horizontal (ground) distance, $\hat{r}_i$, using the known UAV altitude, h. In the (14) converts the estimated 3D slant distance to 2D horizontal distance.

$$\hat{r}_i = \sqrt{\hat{d}_i{}^2 - h^2} \tag{14}$$

The error for a single measurement, e_{ri}, is the difference between the calculated distance from a potential sensor location $[x_s, y_s]$ to a waypoint and the estimated ground distance, $\hat{r}_i$, for that waypoint as (15).

$$r_i - actual = \sqrt{(x_s - x_i)^2 + (y_s - y_i)^2} \tag{15}$$

Where x_i and y_i are the coordinates of the i-th waypoint. In the (16) defines the measurement error.

$$e_{ri} = r_{i-actual} - \hat{r}_i \tag{16}$$

The localization problem is then formulated as an optimization task. The goal is to find the sensor coordinate estimate, $\hat{p}_s$, that minimises the total error across all N waypoints. For this, the multilateration method is used to formulate the objective function. The standard approach is to minimise the sum of the squared errors (SSE), which can be expressed as (17).

$$\hat{p}_s = arg\, min_e(|e_{ri}|) = arg\, min_e \left(\sum_{i=1}^{N} \left(\sqrt{(x_s - x_i)^2 + (y_s - y_i)^2} - \hat{r}_i \right)^2 \right) \tag{17}$$

Where $\hat{p}_s$ is the estimated ground-sensor coordinates $(\hat{x}_s, \hat{y}_s)$.

Since the sensors are in a dense reflective environment, the measured PL is prone to high errors from multipath propagation phenomena. This makes it difficult to find an optimal solution close to the actual location; therefore, powerful optimization algorithms must be utilized. In this work, two distinct algorithms are used to solve the localization problem: WLS and PSO. These two approaches are selected because they combine competitive accuracy with practical implementability under noisy path-loss–derived ranges and multipath reflections. PSO maintains a swarm of candidate solutions and explores multiple regions of the search space simultaneously; candidates that drift towards local minima caused by multipath effects can be guided away through the social and cognitive terms towards fitter regions, which improves robustness on a rough error surface.

In contrast, WLS provides a computationally efficient estimate after linearizing the range equations and incorporates a weighting matrix so that less reliable range estimates contribute less to the final solution. This diversity enables a systematic comparison between a heuristic search method (PSO) and an analytical linearized method (WLS). The following paragraph exhibits the mathematical models of these algorithms.

6.2.1. Particle swarm optimization

PSO explores multiple candidate solutions simultaneously, making it resilient to multipath-induced false minima. For a swarm of M particles let x_k^m and v_k^m be the position and velocity of particle m at iteration k.PSO evolves according to (18).

$$\begin{aligned} v_{k+1}^{(m)} &= \omega v_k^{(m)} + c_1 l_1 \left(p_k^{(m)} - x_k^{(m)}\right) + c_2 l_2 \left(g_k - x_k^{(m)}\right), \\ x_{k+1}^{(m)} &= x_k^{(m)} + v_{k+1}^{(m)}, \end{aligned} \tag{18}$$

Where ω is the inertia weight, $c_1$and c_2 are cognitive and social coefficients respectively, $l_1, l_2 \sim \mathcal{U}(0,1)$ are independent scalars, $\mathrm{p}_k^{(m)} = arg \min_{p \in \{\mathbf{x}_0^{(m)}, \ldots, \mathbf{x}_k^{(m)}\}} \hat{p}$ is particle m's personal best, and $g_k = arg \min_{m \in \{1,..,M\}} f(p_k^{(m)})$ which is the best position found by any particle in the entire swarm up to that point.$f(p)$ is the objective function value at position p.

Boundary conditions (clamping, reflection, or projection) are applied to $x_{k+1}^{(m)}$ to keep particles inside the feasible region. After a determined number of iterations, the global best $g_{k_{final}}$ is reported as the PSO estimate location $\hat{p}_{PSO}$. In summary, for the particle-swarm process, each particle $m = 1, \ldots, M$ at iteration k is characterised by a position vector $x_k^{(m)} \in \mathbb{R}^2$ and a velocity vector$v_k^{(m)}$; the update law contains the inertia weight $\omega \in (0,1]$, which scales the memory of the previous velocity, together with the cognitive and social acceleration coefficients c_1 and c_2 that weight, respectively, the attraction toward the particle's best-ever position $p_k^{(m)}$ and the swarm's global best position g_k. The scalars l_1 and l_2 appearing in the velocity equation are independent draws from the continuous uniform distribution $\mathcal{U}(0,1)$.

6.2.2. Weighted least-squares

WLS reduces the influence of unreliable measurements by weighting them inversely to variance. The WLS algorithm is used to find an analytical solution to the system of non-linear range equations. The equation for each of the N waypoints in a selected group is (19).

$$(\hat{x}_s - x_i)^2 + (\hat{y}_s - y_i)^2 = \hat{r}_i^2 \tag{19}$$

To linearize this system, the equation is expanded and a new variable, $= \hat{x}_s^2 + \hat{y}_s^2$, is introduced. This rearranges the system into the standard linear form $b = Ax$, where $x = [\hat{x}_s, \hat{y}_s, K]^T$ is the vector of unknowns to be solved. The design matrix A and observation vector b are constructed for the *N* waypoints as (20) and (21).

$$A = \begin{bmatrix} 2x_1 & 2y_1 & -1 \\ 2x_2 & 2y_2 & -1 \\ \vdots & \vdots & \vdots \\ 2x_N & 2y_N & -1 \end{bmatrix} \tag{20}$$

$$b = \begin{bmatrix} x_1^2 + y_1^2 - \hat{r}_1^2 \\ x_2^2 + y_2^2 - \hat{r}_2^2 \\ \vdots \\ x_N^2 + y_N^2 - \hat{r}_N^2 \end{bmatrix} \tag{21}$$

The WLS solution incorporates a weight matrix W, where the diagonal entries are typically the inverse of the measurement variance, giving less influence to less reliable data. The solution is given by (22).

$$\hat{x} = (A^T W A)^{-1} A^T W b \tag{22}$$

The final estimated sensor location $[\hat{x}_s, \hat{y}_s]$ is given by the first two elements of the solution vector $\hat{x}$.

6.2.3. Evaluation parameters

The performance of the localization algorithms is evaluated and compared using three standard metrics: the mean absolute error (MAE) and the root-mean-square error (RMSE). These metrics are defined for the set of *S* unknown sensor locations. Let $p = [\hat{x}_s, \hat{y}_s]$ be the true location of sensor *s*, and $\hat{p}_s = [\hat{x}_s, \hat{y}_s]$ be its estimated location. The localization error is the Euclidean distance between these two points, $\|p_s - \hat{p}_s\|$. The metrics are then defined as (23) and (24).

$$MAE = \frac{1}{S}\sum_{s=1}^{S} \|p_s - \hat{p}_s\| \tag{23}$$

$$RMSE = \sqrt{\frac{1}{S}\sum_{s=1}^{S} \|p_s - \hat{p}_s\|^2} \tag{24}$$

MAE averages the absolute deviations and therefore measures the typical linear error magnitude; RMSE squares the deviations before averaging and taking the square root, penalizing larger errors more heavily.

7. SIMULATION ENVIRONMENT SETUP

This section outlines the simulation setup employed to assess the effectiveness of the proposed framework. The simulation setup is partially inspired by [32]. The wireless insite (WI) simulator is used to emulate a realistic UAV-to-ground communication scenario within an urban landscape. The urban region of Rosslyn is selected due to its complex and heterogeneous building structures, which contribute to a multipath-rich propagation environment. The UAV maintains a fixed altitude of 110 m, chosen as a balance between enhancing the probability of line-of-sight (PLOS) connectivity and maximizing ground coverage.

In the simulated environment, 20 ground nodes are randomly distributed across a 400×500 m deployment area. The UAV operates along a predetermined flight path generated using the SCAN algorithm with a 20 m spacing between waypoints, resulting in a total of 546 discrete waypoints. PL estimation is conducted via WI's ray-tracing engine to provide high-fidelity propagation modelling. The key simulation parameters are summarized in Table 2.

Table 2. Environment and simulation parameters

Parameter	Value
Carrier frequency	5.9 GHz
Reference distance d_0	1 m
UAV altitude	110 m
Number of ground nodes	20
Nodes distribution	Random uniform distribution
Deployment area	400×500 m^2
Number of swarm particles	50
Transmit power	10 dBm
Channel bandwidth	500 MHz
Antenna type	Isotropic, gain = 0 dB
Waypoints' spacing	20 m
Number of reflections (max)	6
Number of diffraction (max)	1

8. RESULTS AND DISCUSSION

This section presents and discusses the results obtained from the simulation. It begins by analyzing the characteristics of the simulated PL data, which forms the input for the localization algorithms.

8.1. Path loss analysis

The statistical properties of the PL error, e_k, are first analysed for the N individual measurements. This error is the difference between the measured PL, $PL_{measured,k}$, and the theoretical PL, $PL_{\text{theoretical},k}$, which is the value predicted by the log-distance model using the true distance. In (25) defines the PL error.

$$e_k = PL_{measured,k} - PL_{\text{theoretical},k} \tag{25}$$

From the resulting set of N error values, the mean error, μ_e, is calculated as the arithmetic average. In (26) gives the mean error

$$\mu_e = \frac{1}{N}\sum_{k=1}^{N} e_k \tag{26}$$

The standard deviation of the error, σ_e, which quantifies the spread or variability of the error, is then calculated using the standard formula for an unbiased sample standard deviation. In (27) defines the standard deviation of the error.

$$\sigma_e \sqrt{\frac{1}{N-1}\sum_{k=1}^{N}(e_k - \mu_e)^2} \tag{27}$$

These (25) to (27) provide the mathematical basis for the statistical analysis of the PL measurement errors presented in this work. The distribution of the PL error is shown in Figure 3. The histogram reveals a non-Gaussian, skewed pattern with heavy tails, indicating significant outliers. This broader variability reflects multipath and shadowing-induced fluctuations and underscores the need for further error reduction to improve localization accuracy.

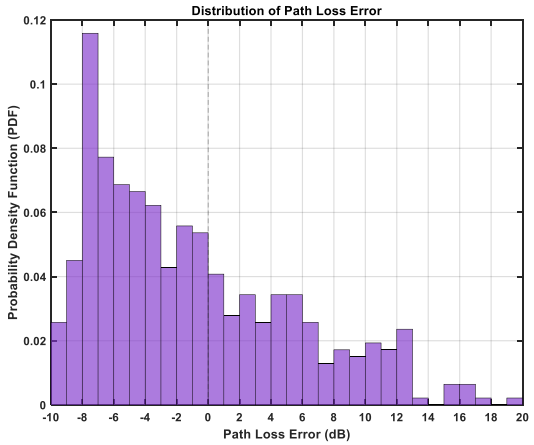

Figure 3. PL errors distribution

To further assess normality, Figure 4 presents a set of diagnostic plots for the linear regression model. The quantile-quantile (QQ) plot in Figure 4(a) compares the empirical residual quantiles against those expected under a Gaussian distribution. While the central portion of the data lies close to the reference line, the systematic divergence in both tails demonstrates clear departures from normality. The upper tail in particular shows extreme deviations, reflecting the influence of large outliers. This behavior is reinforced by the residuals vs fitted plot in Figure 4(b), which shows that the spread of residuals widens systematically as the fitted PL increases. Rather than a constant cloud around zero, the points fan out from a few dB at 93-96 dB to well over 10 dB beyond 101 dB, with several extreme outliers exceeding 30-50 dB. This pattern indicates that the error variance is not constant. Together, these plots provide strong evidence that the residuals cannot be treated as normally distributed and that heavy-tailed effects must be accounted for in robust modelling.

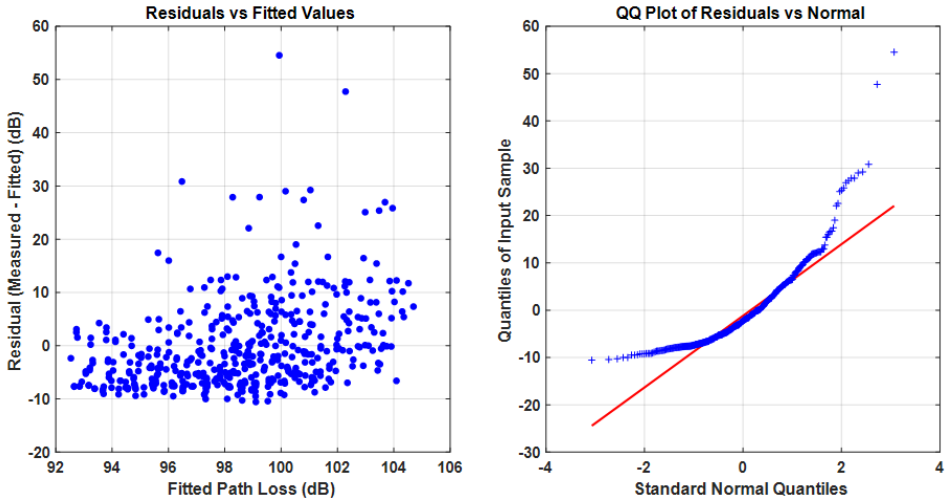

(a) (b)

Figure 4. Linear regression model assumption checks (a) residuals vs fitted value plot and (b) QQ plot of residuals vs normal

Figure 5 visualizes the PL field observed by UAV across the SCAN region for the known reference sensor. Although the transmitter location is fixed, the PL surface is clearly non-uniform due to blockage and multipath in the dense urban layout. This motivates the proposed stage-1 spatial refinement, which reduces local irregularities in the PL samples before estimating PL parameters and performing localization.

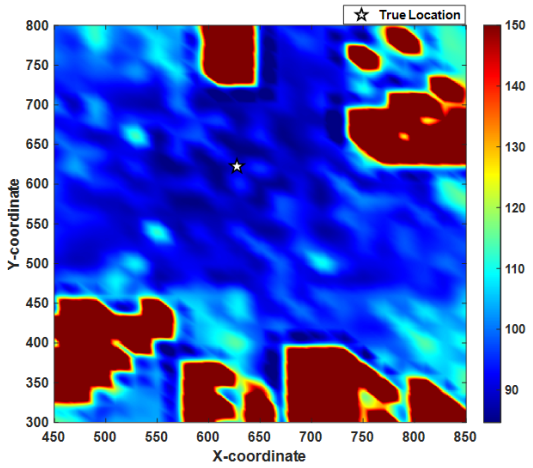

Figure 5. Spatial distribution of PL in the urban SCAN area for the reference sensor

PL values (dB) are obtained from the ray-tracing simulation at the UAV SCAN waypoints and interpolated over the *(x,y)* region for visualization. The star marks the true sensor location. The pronounced spatial fluctuations and localized high-loss regions (e.g., around building blocks) indicate strong NLoS and multipath effects, which can cause large ranging errors if raw PL samples are used directly.

Figure 6 illustrates the effectiveness of the data refining process by comparing the raw PL measurements against the refined PL data. The raw measured data (blue circles) exhibit a significant degree of scatter and contain numerous outliers, such as the measurement above 160 dB, which is characteristic of a multipath-rich environment. In contrast, the spatially refined data (red crosses), using the proposed method described in section 5, is visibly more concentrated around the central trend, showing a clear reduction in variance. This demonstrates that the refining process successfully mitigates the impact of severe outliers and reduces the overall measurement noise. The resulting refined dataset provides a cleaner, more stable input for the subsequent PL model fitting and localization algorithms, as shown by the log-distance fit of the linear model (solid black line).

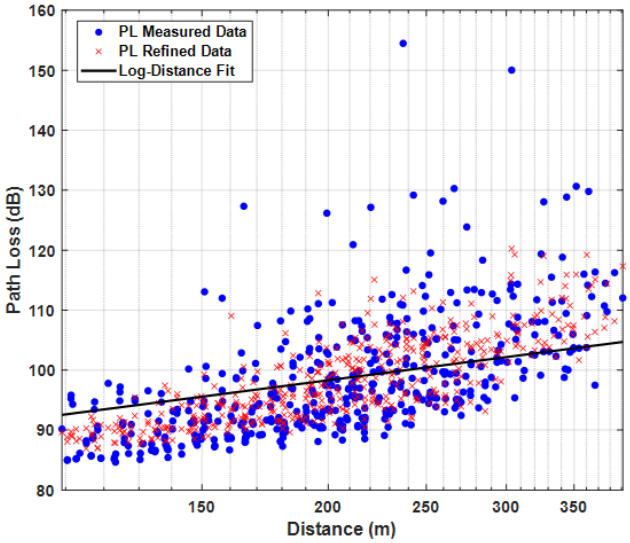

Figure 6. Comparison between PL measured and refined data

8.2. Localization results

This section presents the performance evaluation results for the proposed framework. The evaluation is conducted on the error distribution illustrated in Figure 3. A statistical analysis of this data reveals a high shadowing standard deviation of 8.41 dB. The WLS and PSO localization algorithms are considered to validate the effectiveness of proposed method. Moreover, the obtained results are compared with the baseline approach that uses unprocessed, raw data [33] in terms of MAE and RMSE, as summarized in Table 3.

As illustrated in Table 3, a significant improvement in localization performance was achieved by the proposed method compared with the baseline method. The most dramatic improvement is seen when comparing the "refined data" methods against the "raw data" baseline. Using the raw, unprocessed data resulted in very high localization errors, with an MAE exceeding 150 m. By simply applying the refining process (the "refined data" method), this error was more than halved to approximately 62 m. This proves that mitigating the effects of noise and multipath through data refining is a critical first step for achieving a reasonable level of accuracy, and this reflects on the necessity of data refining.

The most important conclusion is drawn from comparing the "proposed method" against the "refined data" method. While both use refined data, the proposed method adds the crucial step of conditional geometric combination (selecting non-collinear and non-adjacent waypoints), the quantitative impact of which is demonstrated in the detailed analysis in subsection 8.3. This single step reduced the localization error from over 60 m MAE down to 8.5 m MAE, a very high improvement. This demonstrates that simply refining the data is insufficient; the conditional geometric combination of waypoints is the dominant factor in achieving high-precision localization, and this shows critical impact of conditional geometric combination.

The performance of the WLS and PSO algorithms was very competitive. In the "proposed method", PSO achieved a lower error (8.42 m MAE) compared to WLS (8.54 m MAE). This suggests that under conditional geometric combination, both algorithms achieved a similarly accurate localization result.

Table 3. Localization performance comparison

Method	MAE (m)	RMSE (m)
Proposed method (WLS)	8.54	15.28 m
Proposed method (PSO)	8.42	15.08 m
Refined data (WLS)	62.48	65.83 m
Refined data (PSO)	61.41	62.14 m
Raw PL (WLS) [24]	157.71	168.77 m
Raw PL (PSO) [29]	150.92	160.14 m

Figure 7 summarizes localization robustness as the shadowing standard deviation\sigma increases. Raw PL [3] for WLS and [28] for PSO produces very large errors and is highly sensitive to shadowing, and refinement alone improves performance but still leaves substantial error. In contrast, the proposed two-stage method remains consistently low-error for both WLS and PSO, confirming that spatial refinement must be combined with geometry-conditioned subset selection for stable localization in dense urban conditions. The proposed method maintains low and stable localization error across increasing shadowing levels, while raw and refined-only processing exhibit substantially larger RMSE due to multipath/NLoS distortion and weaker geometric conditioning.

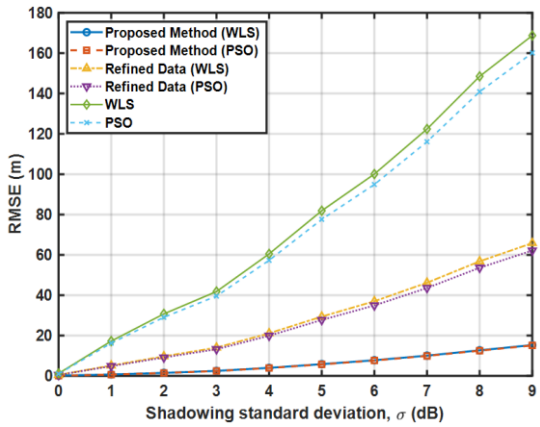

Figure 7. RMSE versus shadowing standard deviation/sigma for WLS and PSO under raw PL, refined PL, and the proposed two-stage framework

8.3. Analysis of the impact of the geometric waypoint

In this analysis, the WLS results are obtained via grid search to find the minimum sum of squared errors. This ensures the optimal solution is found and provides a fair comparison against the PSO algorithm. To analyze the impact of the waypoint geometry on the localization accuracy, four scenarios are considered with different geometric configurations: i) adjacent and non-collinear, ii) collinear and non-adjacent, iii) collinear and adjacent, and iv) non-collinear and non-adjacent. For all scenarios, four waypoints are selected. The distance estimation error at each waypoint is kept constant across the scenarios, with values of +10 m, -7 m, +15 m, and -18 m. The comparative analysis is carried out based on the region of the minimum error surface, which reflects the localization accuracy associated with each geometric configuration.

As illustrated in Figure 8, although the error at each waypoint was kept constant across all scenarios, the region of minimum error on the surface (dark blue area) varies significantly. These results suggest that variation is purely caused by the geometry of the waypoints. It is evident that when waypoints are selected for scenarios 1-3, the area of the minimum error surface region is flat/elongated compared to the area of the region obtained by scenario 4, which utilizes the geometrical conditions mentioned above. These findings highlight that, in scenarios 1-3, the area of global minima is large, making it difficult for localization algorithms to converge on an optimal solution close to the true ground sensor location.

To further analyze the impact of waypoint geometry on localization error, a 50-iteration Monte Carlo simulation was performed for both the WLS and PSO algorithms. In each iteration, the waypoint positions were randomly disturbed while adhering to the geometric constraints of each of the four scenarios. The final localization error was calculated for each run and is illustrated using cumulative distribution function (CDF) in Figure 9. This figure comparing the performance of the four geometric waypoint configurations. The CDF plots for both WLS as in Figure 9(a) and PSO as in Figure 9(b) showed

that the 'non-adjacent, non-collinear (proposed)' geometry configuration significantly improves the localization accuracy compared to the other configurations. In both figures, the curve for the proposed method rises steeply and is furthest to the left, indicating a very high probability of achieving a low localization error. In contrast, the other three geometries show significantly poorer performance, with their curves shifted far to the right, signifying much larger localization errors.

The numerical results from the simulation reinforce these findings. The 'proposed' geometry yielded an exceptionally low average error of approximately 5.9 and 5.8 m for WLS and PSO, respectively. This is an order of magnitude better than the other scenarios, where average errors ranged from 44 m to over 100 m. Notably, the results for the 'proposed' geometry are nearly identical for both algorithms, which demonstrates that when the waypoint geometry is optimal, the localization result is robust and independent of the specific optimization method used.

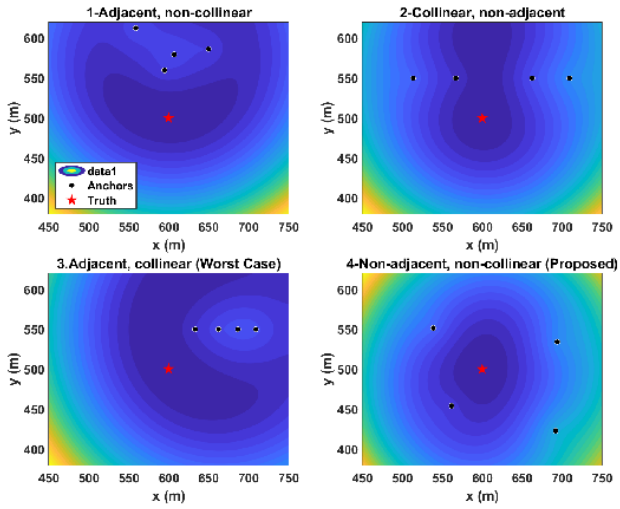

Figure 8. Visualization of the error surface for four different waypoint geometries

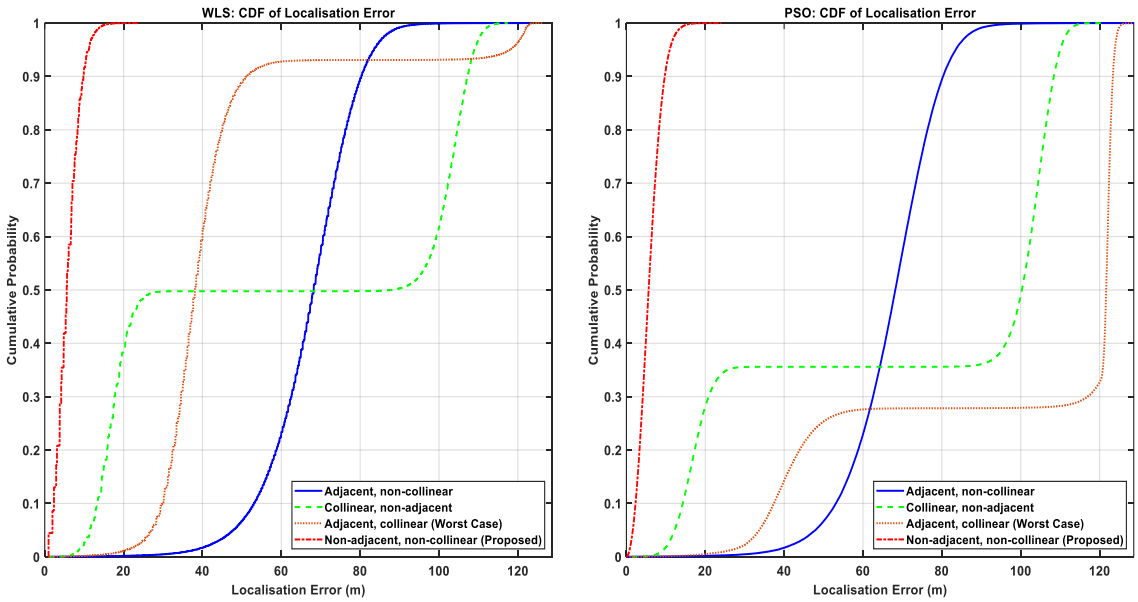

(a) (b)

Figure 9. Cumulative CDF of localization error of (a) WLS and (b) PSO

9. CONCLUSION

In this work, we proposed and validated a two-stage framework for accurate UAV-assisted ground sensor localization in dense urban environments using PL measurements. We demonstrated that processing

raw PL data is insufficient, leading to localization errors exceeding 150 m. The proposed framework addresses this by first refining the PL data. The stage-2 introduces a conditional geometric combination approach to select the non-collinear and non-adjacent waypoints, which proved to be the dominant factor in achieving high accuracy. Unlike prior UAV/RSSI localization studies that rely on fixed PLE assumptions, map-aided LoS/NLoS classification, or direct optimization on raw measurements, our key novelty is the combination of i) spatial PL refinement and ii) conditional geometric subset selection that explicitly rejects near-degenerate waypoint geometries before applying WLS/PSO. Through simulation, we demonstrated that our proposed framework reduced the localization error to ~8.5 m. These findings confirm that data processing and waypoint selection using conditional geometric combination is essential for reliable UAV-based localization in dense multipath scenarios. Practically, the proposed framework enables meter-level UAV-assisted localization in dense urban environments. However, the current results are based on ray-tracing simulations, and the computational load grows with the number of sensors and the waypoint subsets evaluated, which can also increase UAV flight time. The framework is relevant to urban IoT monitoring, post-incident infrastructure/disaster assessment, and asset or sensor tracking in areas where global navigation satellite system GNSS is unreliable. These limitations will be addressed in future work through real-world measurement campaigns and adaptive waypoint/subset and trajectory planning to reduce the required measurements and computation. Future work will evaluate the framework using real-world measurement campaigns in urban environments to validate robustness beyond ray-tracing simulations. In addition, we will explore dynamic 3D UAV trajectories in which altitude is jointly optimized with the horizontal path, and adaptive waypoint planning to reduce the number of measurements while preserving geometric strength. From a scalability perspective, we will investigate how the framework performs as the number of sensors increases, including strategies to reduce computational load through subset pruning and parallel processing, while maintaining accuracy. Finally, integrating 3D urban map awareness into the waypoint-selection stage may further improve reliability under severe NLoS conditions.

FUNDING INFORMATION

This work was supported by the MMU–Naresuan University Matching Grant (MMUE/230045).

AUTHOR CONTRIBUTIONS STATEMENT

This journal uses the Contributor Roles Taxonomy (CRediT) to recognize individual author contributions, reduce authorship disputes, and facilitate collaboration.

Name of Author	C	M	So	Va	Fo	I	R	D	O	E	Vi	Su	P	Fu
Ahmed M. A. A. Elngar	✓	✓	✓	✓	✓	✓	✓	✓	✓	✓	✓	✓	✓	
Heng Siong Lim	✓		✓	✓	✓	✓	✓			✓	✓	✓	✓	✓
Yee Kit Chan					✓		✓			✓				
Yaser Awadh Bakhuraisa	✓	✓	✓	✓	✓	✓		✓	✓	✓	✓		✓	
Ida Wahidah				✓	✓	✓	✓			✓			✓	

C : **C**onceptualization
M : **M**ethodology
So : **So**ftware
Va : **Va**lidation
Fo : **Fo**rmal analysis
I : **I**nvestigation
R : **R**esources
D : **D**ata Curation
O : Writing - **O**riginal Draft
E : Writing - Review & **E**diting
Vi : **Vi**sualization
Su : **Su**pervision
P : **P**roject administration
Fu : **Fu**nding acquisition

CONFLICT OF INTEREST STATEMENT

Authors state no conflict of interest.

DATA AVAILABILITY

The data that support the findings of this study are available from the corresponding author, [LHS], upon reasonable request.

REFERENCES

[1] D. Ebrahimi, S. Sharafeddine, P.-H. Ho, and C. Assi, "Autonomous UAV trajectory for localizing ground objects: a reinforcement learning approach," *IEEE Transactions on Mobile Computing*, vol. 20, no. 4, pp. 1312–1324, 2021, doi: 10.1109/TMC.2020.2966989.

[2] Q. Luo, S. Li, X. Yan, and X. Zhou, "Hierarchical extended Kalman filter cooperative positioning algorithm for UAV swarm," in *2023 IEEE Globecom Workshops (GC Wkshps)*, Dec. 2023, pp. 1801–1806, doi: 10.1109/GCWkshps58843.2023.10464497.

[3] K. N. R. S. V Prasad and V. K. Bhargava, "RSS localization under Gaussian distributed path loss exponent model," *IEEE Wireless Communications Letters*, vol. 10, no. 1, pp. 111–115, Jan. 2021, doi: 10.1109/LWC.2020.3021991.

[4] H. Vo, V. H. L. Nguyen, V. L. Tran, F. Ferrero, F.-Y. Lee, and M.-H. Tsai, "Advance path loss model for distance estimation using LoRaWAN network's received signal strength indicator (RSSI)," *IEEE Access*, vol. 12, pp. 83205–83216, 2024, doi: 10.1109/ACCESS.2024.3412849.

[5] Y. Ding, D. Shen, K. Pham, and G. Chen, "Measurement along the path of unmanned aerial vehicles for best horizontal dilution of precision and geometric dilution of precision," *Sensors*, vol. 25, no. 13, Jun. 2025, doi: 10.3390/s25133901.

[6] V. Teeda, S. Moro, D. Scazzoli, L. Reggiani, and M. Magarini, "Differentiation and localization of ground RF transmitters through RSSI measures from a UAV," *IEEE Transactions on Vehicular Technology*, vol. 74, no. 1, pp. 1000–1009, Jan. 2025, doi: 10.1109/TVT.2024.3458416.

[7] R. J. M. M. Aamir and Z. A. Ali, "UAV-assisted LoRa-based wireless sensor network for environmental monitoring," *Instrumentation*, vol. 12, no. 2, 2025, doi: 10.15878/j.instr.202500294.

[8] S. A. M. Elhassan, N. L. M. Kamal, N. Norhashim, Z. Sahwee, and S. A. Shah, "Unmanned aerial vehicle localisation using RSSI-based trilateration," in *IET Conference Proceedings*, Mar. 2025, vol. 2024, no. 30, pp. 235–240, doi: 10.1049/icp.2025.0261.

[9] Z. Cui *et al.*, "Low-altitude UAV air-ground propagation channel measurement and analysis in a suburban environment at 3.9 GHz," *IET Microwaves, Antennas & Propagation*, vol. 13, no. 9, pp. 1503–1508, Jul. 2019, doi: 10.1049/iet-map.2019.0067.

[10] W. Ahmad, G. Husnain, S. Ahmed, F. Aadil, and S. Lim, "Received signal strength-based localization for vehicle distance estimation in vehicular ad hoc networks (VANETs)," *Journal of Sensors*, vol. 2023, no. 1, Jan. 2023, doi: 10.1155/2023/7826992.

[11] Y. A. Bakhuraisa, A. B. A. Aziz, T. K. Geok, N. B. A. Bakar, and S. B. Jamian, "mm-Wave RSS evaluation for distance estimation in urban environments," in *2022 International Conference on Digital Transformation and Intelligence (ICDI)*, Dec. 2022, pp. 324–329, doi: 10.1109/ICDI57181.2022.10007293.

[12] D. Jin, F. Yin, C. Fritsche, F. Gustafsson, and A. M. Zoubir, "Bayesian cooperative localization using received signal strength with unknown path loss exponent: message passing approaches," *IEEE Transactions on Signal Processing*, vol. 68, pp. 1120–1135, 2020, doi: 10.1109/TSP.2020.2969048.

[13] L. A. C. Najarro, I. Song, S. Tomic, and K. Kim, "Fast localization with unknown transmit power and path-loss exponent in WSNs based on RSS measurements," *IEEE Communications Letters*, vol. 24, no. 12, pp. 2756–2760, Dec. 2020, doi: 10.1109/LCOMM.2020.3016710.

[14] Y. Li, B. Mukhopadhyay, and M.-S. Alouini, "RSS-based cooperative localization and transmit power(s) estimation using mixed SDP-SOCP," *IEEE Transactions on Vehicular Technology*, vol. 72, no. 12, pp. 16936–16941, Dec. 2023, doi: 10.1109/TVT.2023.3295868.

[15] Y. Li, B. Mukhopadhyay, J. Xu, and M.-S. Alouini, "Experimental validation of cooperative RSS-based localization with unknown transmit power, path loss exponent, and precise anchor location," *IEEE Transactions on Wireless Communications*, vol. 23, no. 11, pp. 16482–16497, Nov. 2024, doi: 10.1109/TWC.2024.3441643.

[16] B. Liu, X. Zhu, Y. Jiang, Z. Wei, and Y. Huang, "UAV and piecewise convex approximation assisted localization with unknown path loss exponents," *IEEE Transactions on Vehicular Technology*, vol. 68, no. 12, pp. 12396–12400, Dec. 2019, doi: 10.1109/TVT.2019.2946142.

[17] X. Cheng *et al.*, "Communication-efficient coordinated RSS-based distributed passive localization via drone cluster," *IEEE Transactions on Vehicular Technology*, vol. 71, no. 1, pp. 1072–1076, Jan. 2022, doi: 10.1109/TVT.2021.3125361.

[18] Y. Li, F. Shu, B. Shi, X. Cheng, Y. Song, and J. Wang, "Enhanced RSS-based UAV localization via trajectory and multi-base stations," *IEEE Communications Letters*, vol. 25, no. 6, pp. 1881–1885, Jun. 2021, doi: 10.1109/LCOMM.2021.3061104.

[19] Y. Chu, W. Guo, K. You, L. Zhao, T. Peng, and W. Wang, "RSS-based multiple co-channel sources localization with unknown shadow fading and transmitted power," *IEEE Transactions on Vehicular Technology*, vol. 71, no. 12, pp. 13344–13355, Dec. 2022, doi: 10.1109/TVT.2022.3201447.

[20] Q. Wang, Z. Duan, and F. Li, "Semidefinite programming for wireless cooperative localization using biased RSS measurements," *IEEE Communications Letters*, vol. 26, no. 6, pp. 1278–1282, Jun. 2022, doi: 10.1109/LCOMM.2022.3166780.

[21] V. Kumar, R. Arablouei, R. Jurdak, B. Kusy, and N. W. Bergmann, "RSSI-based self-localization with perturbed anchor positions," in *2017 IEEE 28th Annual International Symposium on Personal, Indoor, and Mobile Radio Communications (PIMRC)*, Oct. 2017, pp. 1–6, doi: 10.1109/PIMRC.2017.8292600.

[22] S. Hu, L. Guo, Z. Liu, and S. Gao, "Multipath-assisted ultra-wideband vehicle localization in underground parking environment using ray-tracing," *Sensors*, vol. 25, no. 7, Mar. 2025, doi: 10.3390/s25072082.

[23] B. Yang, L. Guo, R. Guo, M. Zhao, and T. Zhao, "A novel trilateration algorithm for RSSI-based indoor localization," *IEEE Sensors Journal*, vol. 20, no. 14, pp. 8164–8172, Jul. 2020, doi: 10.1109/JSEN.2020.2980966.

[24] S. Kang, T. Kim, and W. Chung, "Hybrid RSS/AOA localization using approximated weighted least square in wireless sensor networks," *Sensors*, vol. 20, no. 4, Feb. 2020, doi: 10.3390/s20041159.

[25] O. Esrafilian, R. Gangula, and D. Gesbert, "UAV-aided wireless node localization using hybrid radio channel models," in *2022 IEEE International Conference on Communications Workshops (ICC Workshops)*, May 2022, pp. 1083–1088, doi: 10.1109/ICCWorkshops53468.2022.9814677.

[26] O. Esrafilian, R. Gangula, and D. Gesbert, "Three-dimensional-map-based trajectory design in UAV-aided wireless localization systems," *IEEE Internet of Things Journal*, vol. 8, no. 12, pp. 9894–9904, 2021, doi: 10.1109/JIOT.2020.3021611.

[27] W. Zhang and W. Zhang, "An efficient UAV localization technique based on particle swarm optimization," *IEEE Transactions on Vehicular Technology*, vol. 71, no. 9, pp. 9544–9557, Sep. 2022, doi: 10.1109/TVT.2022.3178228.

[28] Q. Yang, "A new localization method based on improved particle swarm optimization for wireless sensor networks," *IET Software*, vol. 16, no. 3, pp. 251–258, Jun. 2022, doi: 10.1049/sfw2.12027.

[29] D. Koutsonikolas, S. M. Das, and Y. C. Hu, "Path planning of mobile landmarks for localization in wireless sensor networks," *Computer Communications*, vol. 30, no. 13, pp. 2577–2592, Sep. 2007, doi: 10.1016/j.comcom.2007.05.048.

[30] I. Remcom, *Wireless insite reference manual*, Version 2.8.1, Remcom, Inc. Manual, 2016.

[31] S. Coene *et al.*, "Path loss modeling for air-to-ground channels in a suburban environment," in *2024 18th European Conference on Antennas and Propagation (EuCAP)*, Mar. 2024, pp. 1–5, doi: 10.23919/EuCAP60739.2024.10501506.

[32] Y. Bakhuraisa, H. S. Lim, Y. K. Chan, and M. Hilman, "UAV-assisted localization of ground nodes in urban environments using path loss measurements," *Drones*, vol. 9, no. 6, Jun. 2025, doi: 10.3390/drones9060450.

[33] Y. Sung, "RSSI-based distance estimation framework using a Kalman filter for sustainable indoor computing environments," *Sustainability*, vol. 8, no. 11, Nov. 2016, doi: 10.3390/su8111136.

BIOGRAPHIES OF AUTHORS

Ahmed M. A. A. Elngar received the B.Eng. degree in Electronic Engineering and Computer Science from Satya Wacana Christian University (UKSW), Indonesia in 2022. Currently, he is pursuing a Master of Engineering Science at the Faculty of Engineering and Technology (FET), Multimedia University, Malaysia. His research interests include localization, WPT and PLS. He can be contacted at email: ahmedelngar02@gmail.com.

Heng Siong Lim received the B.Eng. degree (Hons.) in Electrical Engineering from the Universiti Teknologi Malaysia, Malaysia, in 1999, and the M.Eng.Sc. and Ph.D. degrees in Wireless Communications from Multimedia University, Malaysia, in 2002 and 2008, respectively. He is currently a professor at the Faculty of Engineering and Technology, Multimedia University, Malaysia. His research interests include the areas of signal processing for wireless communications and advanced digital communication receiver's design. He is senior member of IEEE. He can be contacted at email: hslim@mmu.edu.my.

Yee Kit Chan received his B.Eng. (Hons) in Electrical Engineering from the University of Malaya. He obtained his M.Eng.Sc. and Ph.D. in Microwave Engineering from the Multimedia University, Malaysia. He is currently a professor at the Faculty of Engineering and Technology, Malaysia. He is a registered professional engineer with the board of engineers Malaysia and a professional technologist with the malaysia board of technologists. His research interests include synthetic aperture radar design, microwave remote sensing, radar sensor development and RF system design. He is presently chair of the IEEE Geoscience and Remote Sensing Society Chapter, Malaysia Section. In 2021, he was awarded the top research scientist Malaysia (TRSM) by the Academy of Sciences Malaysia (ASM) and admitted as a fellow of the ASEAN Academy of Engineering and Technology in 2022. He is also listed in vol 1, 2022 of "who's who in engineering Malaysia" published by the Board of Engineers Malaysia. He can be contacted at email: ykchan@mmu.edu.my.

Yaser Awadh Bakhuraisa received his B.Eng. in Electronic Engineering from Hadhramout University of Science and Technology, Hadhramout, Yemen, in 2009, and his M.Eng. in Electronic Engineering (Electronic Systems) from Universiti Teknikal Malaysia Melaka (UTeM), Malaysia, in 2019. He is currently a member of the academic staff at Seiyun Community College, Hadhramout, Yemen. He is pursuing a Ph.D. at Multimedia University, Malaysia in the fields of vehicular detection and localization for intelligent transportation systems. His research interests include vehicular communication, radio propagation, and machine learning. He can be contacted at email: yasser.awad480@gmail.com.

Ida Wahidah received the B.Eng. and M.Eng. degrees in Electrical Engineering from Institut Teknologi Bandung, Indonesia in 2005, and the Ph.D. degree in Electrical and Informatics Engineering from the same university in 2014. She is currently an associate professor at the School of Electrical Engineering, Telkom University, Indonesia. She was the head of Networks and Multimedia Expertise Group until 2010, and chair of the graduate Department of Electrical Engineering since 2020. In 2015-2016, she spent time in industrial research under Markany funding, South Korea. Since 2016, she has received various national and international research grants. Her research interests focus on wireless body sensor networks, network security, video watermarking, and compressed sensing applications. She is also a consultant in telecommunication interconnection regulation. She can be contacted at email: wahidah@telkomuniversity.ac.id.